

# Commercial CMOS Foundry Thermal Display for Dynamic Thermal Scene Simulation

Michael Gaitan, M. Parameswaran\*, R. Barry Johnson\*\*, and Ronald Chung\*\*

National Institute of Standards and Technology,<sup>1</sup> Gaithersburg, MD 20899

\*Simon Fraser University, Burnaby, BC, Canada V5A 1S6

\*\*Optical E.T.C., Inc., 3077 Leeman Ferry Road, Huntsville, AL 35801

*Abstract:* We report on the performance of a flat-panel thermal display technology, prototype developed at NIST in collaboration with Simon Fraser University and Optical E. T. C., for dynamic thermal scene simulation (DTSS). The pixel elements of the display are composed of thermally-isolated resistive heaters. The main innovation is the fabrication method which uses commercial CMOS integrated circuit (IC) foundries. This method produces a low-manufacturing-cost, high-yield, thermal display technology. Circuits for drive and control are monolithically integrated on the display. The microheating element has a thermal time constant of a few milliseconds and a temperature range of operation from ambient to over 1000 °C. A 16x16 pixel array with a 0.2-mm pixel pitch is presented as a demonstration of the concept; however, the circuit design supports larger sizes (e.g. 256x256). This display technology is compatible with DTSS requirements for laboratory and fieldable built-in test/built-in test equipment (BIT/BITE) applications.

## Introduction

The continuing improvements in infrared (IR) imaging technology and its use in weapons and surveillance systems, and more recently, in industrial applications require new technology and procedures for testing and calibration. For example, an IR imager may be used as a component for the lock-in and guidance of a complex and costly weapons system. Traditional testing techniques using blackbody radiation from static thermal targets is not sufficient. Thermal displays that can generate temporal thermal scenes are also needed [1].

For the present, laboratory testing of "hardware in the loop" simulations requires these displays for characterization not only of the imaging system, but also for testing the software and hardware components that make up the entire guidance system. These tests expose the imaging and guidance system to real-time scenarios, and the response of the system can be evaluated.

Similar tests will be needed in the field. Furthermore, a field test that will give a simple pass/fail criterion may not be enough. Performance data measured over time may be necessary as a means for the prediction of failures and for maintenance scheduling. Since these tests can be quite complicated, the cost of logistics support can be lessened if the test can be automated and carried out quickly, and if the test target can be built into the system to provide a self-test/self-calibration function. In some cases, e.g., the deployment of an IR imaging system in space, the test must be built into the system since access will not be feasible. DTSS for field testing will only be possible if the cost of manufacturing thermal displays is cheap enough, and if the display is small, light, and consumes little power.

Thermal displays consisting of microheating elements that are fabricated using an IC-based manufacturing process have been identified as the best solution for thermal scene simulation requirements [2]. In general, an IC-based microheating element can be fabricated by surface micromachining techniques either by bulk silicon micromachining [3,4,5] or by the removal of a sacrificial layer [6,7]. The purpose of the micromachining step is to provide the necessary thermal isolation by forming a suspended heating element. We refer to the prevalent methods for fabricating micromechanical elements as full custom fabrication; i.e., the fabrication process sequence deviates from a standard IC foundry process.

---

<sup>1</sup>Contribution of the National Institute of Standards and Technology; not subject to copyright. In this report, commercial equipment, instruments, and computer programs may be identified to specify the procedure adequately. This does not imply recommendation or endorsement by NIST, nor does it imply that the equipment or program is the best available for the purpose.

Devices that can be fabricated using a commercial IC foundry as compared to full custom fabrication can be expected to be less expensive because of the economies of scale. In this paper we report on the performance of microheating elements for thermal displays fabricated by using a commercial CMOS foundry and a post-CMOS-fabrication, or post-fabrication, etch process. We refer to this fabrication method as the CMOS-compatible micromachining technique.

### CMOS-Compatible Microheaters

The CMOS-compatible micromachining technique [8] is based a computer-aided design (CAD) procedure that utilizes a newly defined layer that we call *open* [9]. The *open* layer in the CAD layout represents an opening in the SiO<sub>2</sub> passivation layers of a IC that exposes the silicon surface. The opening is formed with no additional photolithography steps; it is the combination of all the contact cuts in a standard CMOS process (substrate contact, polysilicon contact, metal contact, and glass cut for the bonding pad). This opening allows the anisotropic etchant used in the post-fabrication process step, EDP [10], to create a pit by etching the silicon substrate. The SiO<sub>2</sub> passivation layers, present over the entire surface except over the *open* areas and over the bond pads, act as the mask for the etchant. By a proper choice of the layout pattern, a suspended membrane consisting of SiO<sub>2</sub>, polysilicon, and aluminum can be created. Recently, the *open* layer was incorporated in the technology file for MAGIC [11], a popular public-domain design software. This implementation has now been added to the MOSIS [12] SCMOS technology file [13].

Figure 1 shows a scanning electron microscope (SEM) micrograph of a microheater element fabricated using this technique. This device was first reported in [14] for the application as an IR point source for DTSS. The heater is formed over a 150x150- $\mu$ m pit. The microheater is composed of a polysilicon layer for the heating element, aluminum lines for electrical contact, and glass passivation that encapsulates the heater and provides the mechanical support. The pit forms an inverted pyramid cavity, and the heating element is shaped like a trampoline with four support beams. The four surfaces of the pit are defined by <111> planes of the silicon crystal lattice and form an angle of 54.7° from the top surface. For a review of silicon micromachining technology, one can refer to [15].

Figure 2 is a plot of the temperature of the microheating element as a function of input power. The temperature of the element is shown to vary from ambient to 500 °C with a thermal efficiency of 37.5 °C/mW. The temperature is calculated by using the resistance of the heating element and its thermal coefficient of resistance [16]. The thermal

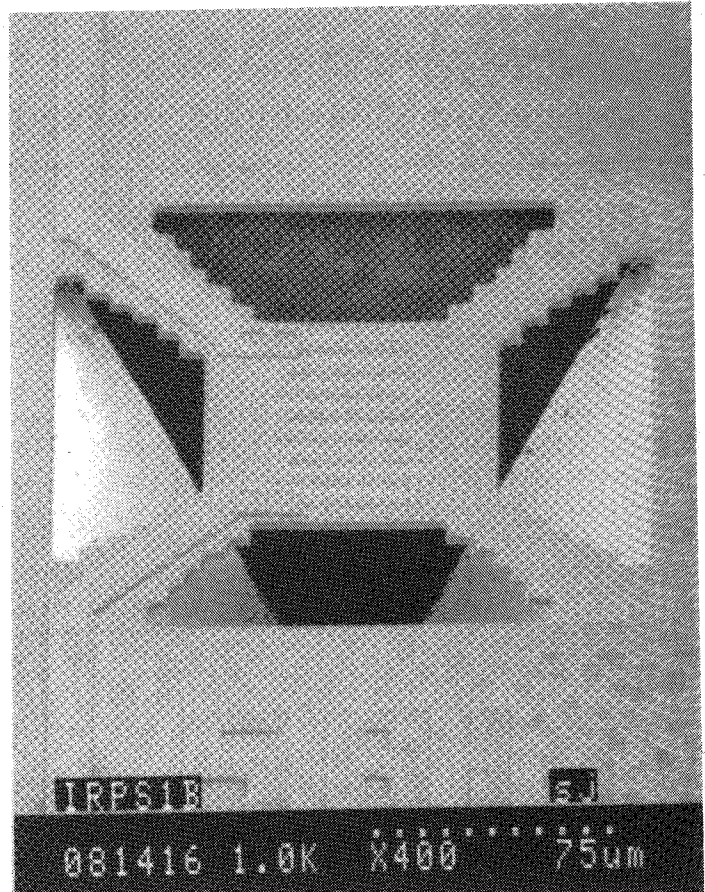


Figure 1 SEM micrograph of microheating element (thermal pixel).

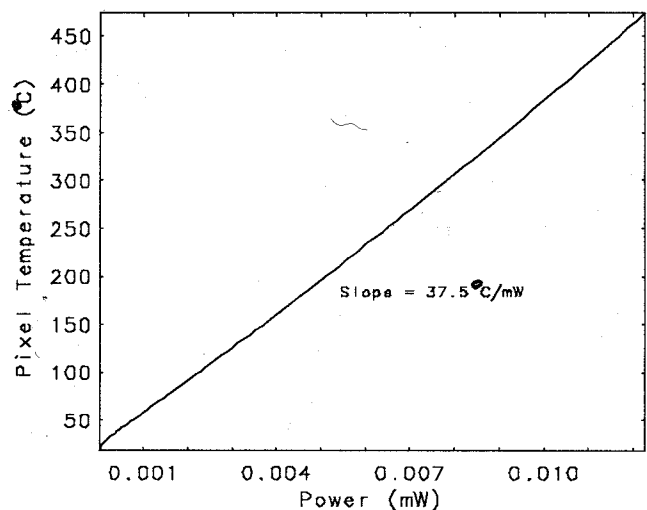
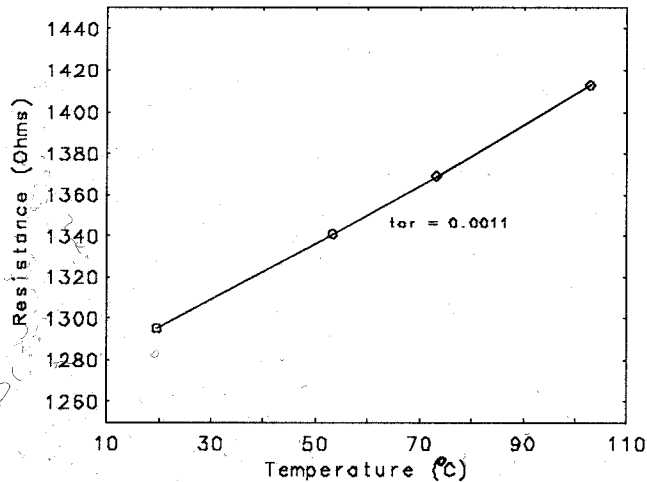
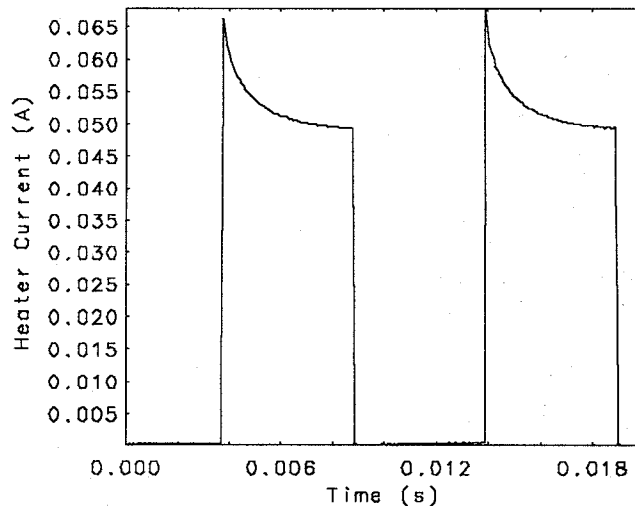


Figure 10 Plot of thermal pixel temperature vs. power dissipation in the heating element.



**Figure 2** Plot of heater resistance vs. temperature of heater. The TCR is defined as  $(R-R_0)/R_0$  where  $R_0$  is the resistance at room temperature.



**Figure 4** Plot of transient current of microheating element.

coefficient of resistance is measured to be  $0.003/^{\circ}\text{C}$  as shown in figure 3. This parameter is used to extrapolate the temperature at higher power dissipations. Earlier work used this effect of temperature on resistance as a means to sense gas flow [17].

Figure 4 is a photograph of the device operating in incandescence demonstrating the temperature range of operation of the heating element from ambient to over  $1000^{\circ}\text{C}$ . Figure 5 is a plot of the transient response of the heater current to a voltage pulse. As can be seen, the current starts at a higher level (resistor temperature is initially at ambient), and increases to an equilibrium value as the temperature reaches a steady state. The figure also demonstrates that the thermal time constant is on the order of 1 ms. This type of pulse testing was used to measure the stability of the microheating elements. A 100-Hz pulse frequency was chosen so that the heating elements underwent a complete thermal cycle from ambient to operating temperature. Figure 6 shows the results of the stress test where the heating element was cycled 1 billion

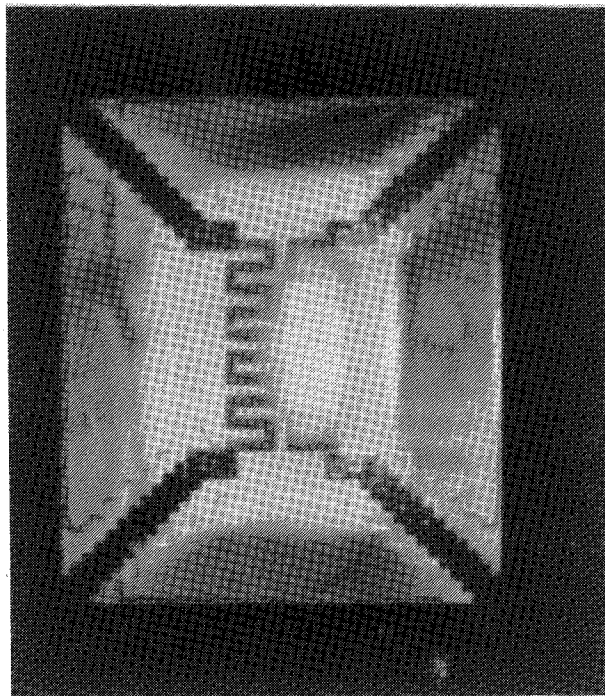


**Figure 3** Photomicrograph of the microheating element operating in incandescence. The device is supplying its own illumination.

Figure 5 is a plot of the resistance of the heating element over time for pulsed stress testing. The graph shows Resistance (Ohms) on the y-axis (700 to 880) and Time (s) on the x-axis (log scale from  $10^0$  to  $10^8$ ). The resistance increases from ~700 Ohms at  $10^0$  s to ~880 Ohms at  $10^8$  s.

**Figure 5** Plot of the resistance of the heating element over time for pulsed stress testing.

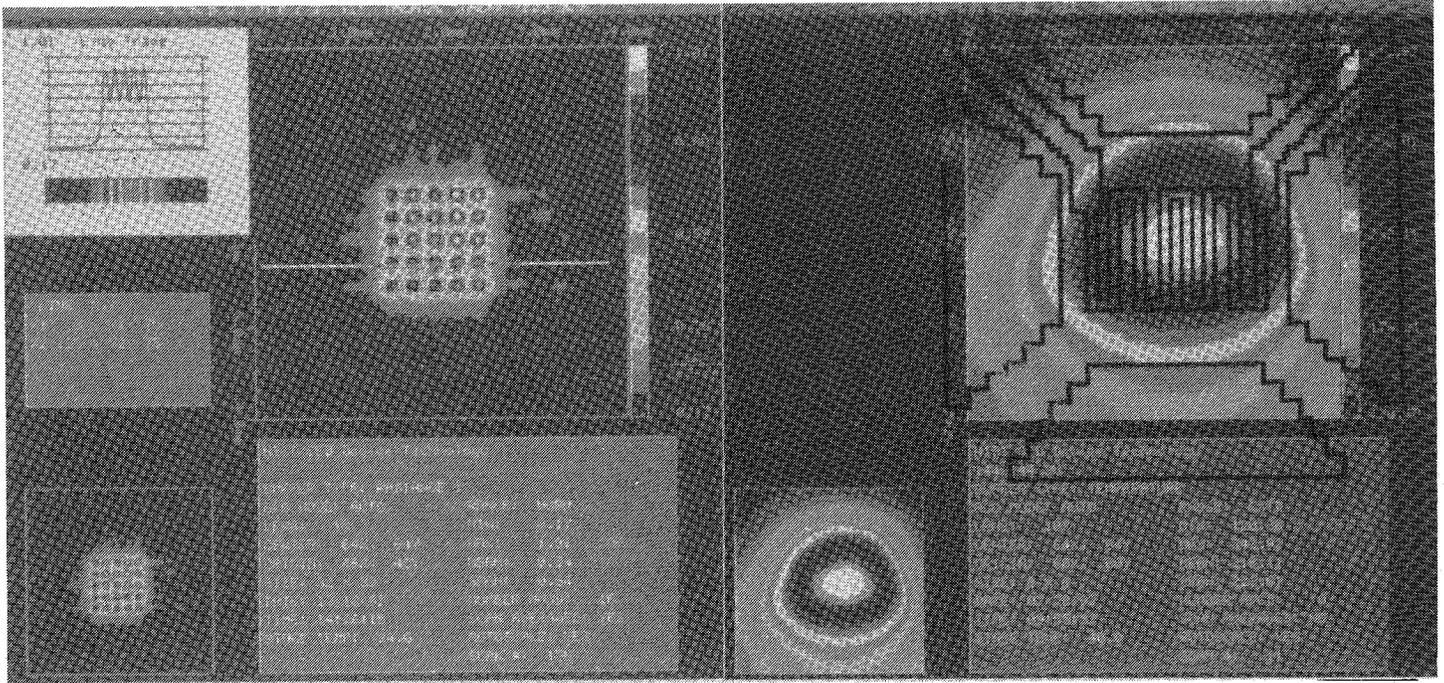


**Figure 6** Two-dimensional plot of radiance of an array of microheating elements.

**Figure 7** A 2-dimensional plot of microheater temperature calculated using radiance measurements.

times. This test was carried out under conditions where the on-state voltage was constant during the experiment. Other stress tests carried out under constant current and constant power conditions are still underway. Some noise in the data is attributed to thunderstorms and other interruptions because of the time that the experiment took to complete (an entire summer). As can be seen in the figure, the resistance increases logarithmically over time. This resistance increase is acceptable. After a burn-in, the resistance change over time can be stabilized. The display can also be calibrated for temperature uniformity in the presence of some resistance variations. Some new designs for the heater elements are in progress that further increase the stability of the heating elements.

### Spectral Response Measurements

An initial evaluation of the spectral emissivity of a typical thermal pixel element has been made. The emitted flux from the pixel was measured over six different spectral ranges within the 2- to 14- $\mu\text{m}$  spectrum. The infrared detector-filter assembly was calibrated against a known blackbody source. By utilizing dual spectral-band radiometric techniques [18], the emissivity within several bands was calculated from the measured data. When the pixel's apparent temperature was about 300  $^{\circ}\text{C}$ , the relative emissivities were 1.00, 0.56, and 0.70 in the 2.5- to 4.0- $\mu\text{m}$ , 4- to 6- $\mu\text{m}$ , and 6- to 14- $\mu\text{m}$  spectral bands, respectively. Since the temperature was not uniform over the heater element, the absolute emissivity could not be exactly measured with the experimental arrangement used. Based on these considerations, the emissivity in the 2- to 4- $\mu\text{m}$  spectral band is thought to be about 0.8. Consequently, the emissivity of the thermal pixel is in a practical range.

Measurements of radiance and temperature were also carried out. Figure 7 shows two-dimensional plot of radiance of an array of heating elements. Radiance measurements were used to estimate the temperature contours of the microheater. Figure 8 shows a two-dimensional plot of temperature of a single microheating element.

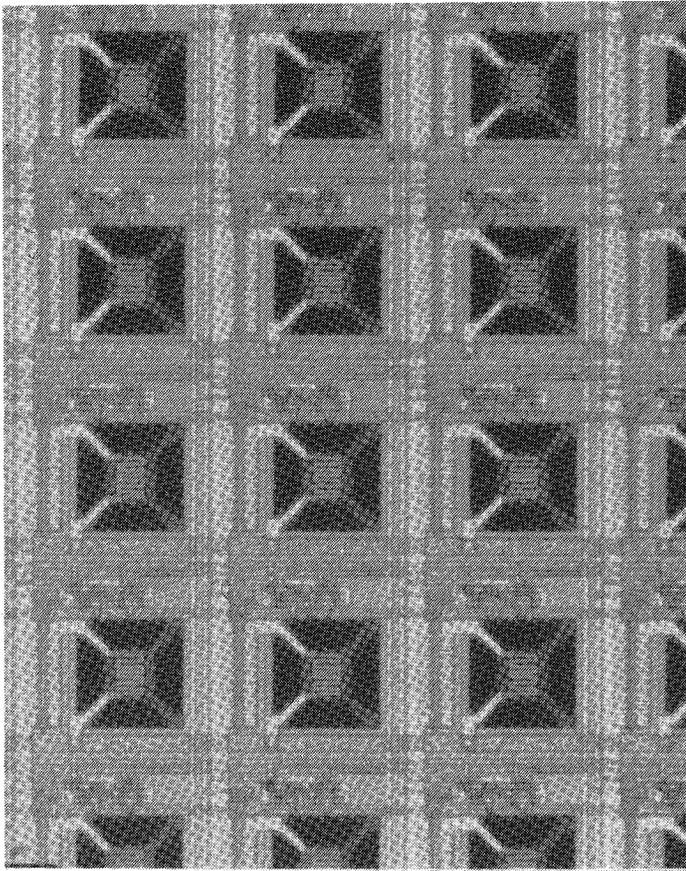


Figure 8 Photomicrograph of a small section of the CMOS foundry-fabricated 16x16 thermal display.

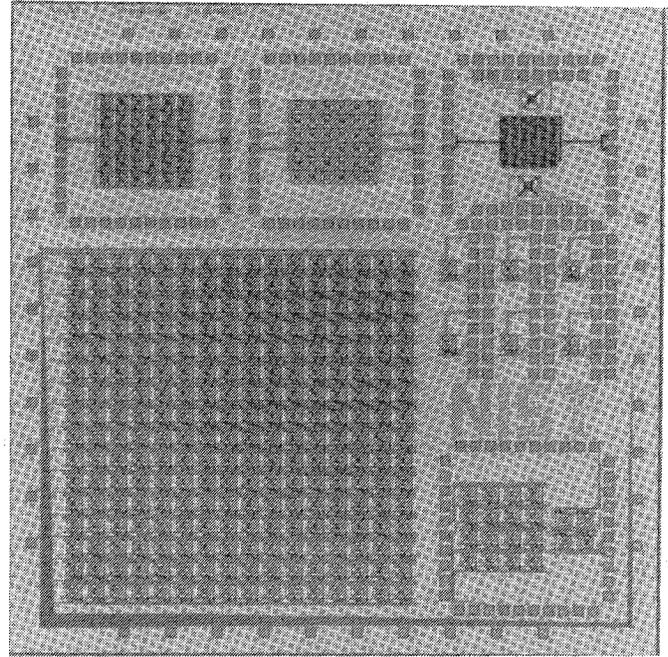


Figure 9 Photograph of the IC chip containing the 16x16 pixel CMOS-foundry-fabricated thermal display.

### Thermal Display Demonstration

Figure 9 shows a photograph of a section of a 16x16 pixel thermal display with thermal pixel elements integrated with control circuitry (pixel pitch is 0.2 mm). The display is fabricated using a standard 2- $\mu$ m CMOS foundry process available through the MOSIS service. It has already been demonstrated that circuits fabricated in the CMOS process are, in general, not degraded by the post-fabrication procedure [19]. Circuit integration with micromachined thermal heating elements has been reported in [20,21]. Figure 10 shows a photograph of the IC chip containing the 16x16 pixel thermal display. Each pixel has circuitry for row and column select, enable, analog pass gate, and drive transistor. The pass gate can hold the analog signal for many seconds, even when the microheating element temperature is hundreds of  $^{\circ}$ C.

Measurements of array uniformity show a 1% standard deviation from the mean heater resistance. Yield of the micromachined elements is also high. Virtually all the devices work; nonfunctional devices have for the most part been traced to a design error. Simple computer controlled scenes such as single lighted pixels moving in random directions have been demonstrated with the 16x16 array. Demonstration of sophisticated scene simulation awaits the 256x256 pixel displays.

### Conclusions

A display technology was presented that is manufacturable using commercial CMOS IC foundries. Silicon micromachining realizes tiny thermally isolated micro-heaters that are integrated with CMOS electronics for drive and control of the display. The manufacturing technique leads to low-cost foundry-independent technology. This display technology is appropriate for laboratory testing and for built-in test/built-in test equipment (BIT/BITE) logistics support for field testing of IR-based tracking, guidance, and surveillance systems.

Results were reported on thermal pixel design, fabrication, thermal measurements, reliability studies, pixel uniformity, spectral response, and comparisons to black body radiators. The pixel elements are 150  $\mu\text{m}$  in size. Pixel temperature can be varied from ambient to 1000  $^{\circ}\text{C}$  with 24-mW power and a thermal response time of 1 ms. These results show that this display technology will satisfy thermal scene simulation requirements.

Circuitry for array operation using digital and analog control of pixel temperature has been designed and tested. A thermal display with a 16x16 pixel array has been fabricated, and the operation of the 16x16 array was discussed. All circuitry is modular and current designs are easily expandable to 256x256 arrays.

### Acknowledgments

The first two authors thank Jon Geist for the initial conception of applying the CMOS-compatible micromachining technique to fabricate thermal display pixels for dynamic thermal scene simulation, and for initiating projects leading to the results reported here.

This work was supported by the Navy Advanced Test Equipment and Metrology (ATE/M) Project at NRAD and by the Army Test Measurements and Diagnostic Equipment (TMDE) Activity at Redstone Arsenal.

### References

- [1] A. P. Pritchard, "Dynamic IR Scene Generation: Basic Requirements and Comparative Display Design," *Proc. SPIE*, vol. 940, pp. 144-149, 1988.
- [2] T. Barnett, "IR Transducer Technology: An Overview," *Proc. SPIE*, vol. 765, pp. 82-84, 1987.
- [3] M. Daehler, "Infrared Display Array," *Proc. SPIE*, vol. 765, pp. 82-84, 1988.
- [4] E. Yoon and K. Wise, "An Integrated Mass Flow Sensor with On-Chip CMOS Interface Circuitry," *IEEE Trans. Elec. Dev.*, vol. 39, no. 6, pp. 1376-1386, 1992.
- [5] K. R. Williams and R. S. Muller, "IC-Processed Hot-Filament Vacuum Microdevices," *IEDM Technical Digest*, pp. 387-389, San Francisco, CA, December 13-16, 1992.
- [6] R. A. Wood, C. J. Han, and P. W. Kruse, "Integrated Uncooled Infrared Detector Imaging Arrays," *Proc. IEEE Solid-State Sensor and Actuator Workshop*, pp. 132-135, Hilton Head Island, South Carolina, June 22-25, 1992.
- [7] R. T. Howe, "Surface Micromachining for Microsensors and Microactuators," *J. Vac. Sci. Technol. B*, vol. 6, no. 6, pp. 1809-1813, 1988.
- [8] M. Parameswaran, H. P. Baltes, Lj. Ristic, A. C. Dhaded, and A. M. Robinson, "A New Approach for the Fabrication of Micromechanical Structures," *Sensors and Actuators*, vol. 19, pp. 289-307, 1989.
- [9] J. C. Marshall, M. Parameswaran, M. E. Zaghoul, and M. Gaitan, "High-Level CAD Melds Micromachined Devices with Foundries," *IEEE Circuits and Devices*, vol. 8, no. 6, pp. 10-17, November 1992.
- [10] R. M. Fine and D. L. Klein, "A water-amine-complexing agent system for etching silicon," *J. Electrochem. Soc.*, vol. 114, p. 965, 1967.
- [11] J. K. Ousterhout, "The User Interface and Implementation of an IC Layout Editor," *IEEE Trans. CAD*, vol. 3, no. 3, 1984.
- [12] C. Tomovich, "MOSIS - A Gateway to Silicon," *IEEE Circuits and Devices*, vol. 4, no. 2, 1988.

- [13] Jen-I Pi and Shih-Lien Lu, "Magic Technology Manual for MOSIS Scalable CMOS," *USC/ISI Technical Report*, To be Published.
- [14] M. Parameswaran, A. M. Robinson, D. L. Blackburn, M. Gaitan, and J. Geist, "Micromachined Thermal Radiation Emitter from a Commercial CMOS Process," *IEEE Electron Device Letters*, 12 (2), pp. 57-59, 1990.
- [15] K. E. Peterson, "Silicon as a Mechanical Material," *Proc. IEEE*, vol. 70, no. 5, pp. 420-457, 1982.
- [16] H. A. Schafft and J. S. Suehle, "The Measurement, Use and Interpretation of the Temperature Coefficient of Resistance of Metallizations," *Solid-State Electronics*, vol. 35, no. 3, pp. 403-410, 1992.
- [17] M. Parameswaran, a. M. Robinson, Lj. Ristic, K. Chau, and W. Allegretto, "A CMOS thermally isolated gas flow sensor," *Sensors and Materials*, vol. 19, pp. 289-307, 1989
- [18] D. Fehribach and R. B. Johnson, "Temperature Measurement Validity for Dual Spectral-Band Radiometric Techniques," *Opt. Eng.*, vol. 28, no. 12, pp. 1255-1259, 1989.
- [19] R. Chung, "Control Electronics for Array of Blackbody Silicon Emitters," Thesis, Simon Fraser University, 1991.
- [20] M. Parameswaran, R. Chung, M. Gaitan, R. B. Johnson, and M. Syrzycki, "Commercial CMOS Fabricated Integrated Dynamic Thermal Scene Simulator," *IEDM Technical Digest*, pp. 753-756, 1991.
- [21] M. Gaitan, M. Parameswaran, M. Zaghoul, J. Marshall, B. Novotny, and J. Suehle, "Design Methodology for Micromachanical Systems at Commercial CMOS Foundries Through MOSIS," *Proc. 35<sup>th</sup> Midwest Symposium on Circuits and Systems*, Washington DC, August 1992.